

# A Versatile Route to Assemble Semiconductor Nanoparticles into Functional Aerogels by Means of Trivalent Cations

Dániel Zámbo, Anja Schlosser, Pascal Rusch, Franziska Lübke, Julian Koch, Herbert Pfnür, and Nadja C. Bigall\*

3D nanoparticle assemblies offer a unique platform to enhance and extend the functionality and optical/electrical properties of individual nanoparticles. Especially, a self-supported, voluminous, and porous macroscopic material built up from interconnected semiconductor nanoparticles provides new possibilities in the field of sensing, optoelectronics, and photovoltaics. Herein, a method is demonstrated for assembling semiconductor nanoparticle systems containing building blocks possessing different composition, size, shape, and surface ligands. The method is based on the controlled destabilization of the particles triggered by trivalent cations ( $Y^{3+}$ ,  $Yb^{3+}$ , and  $Al^{3+}$ ). The effect of the cations is investigated via X-ray photoelectron spectroscopy. The macroscopic, self-supported aerogels consist of the hyperbranched network of interconnected CdSe/CdS dot-in-rods, or CdSe/CdS as well as CdSe/CdTe core-crown nanoplatelets is used to demonstrate the versatility of the procedure. The non-oxidative assembly method takes place at room temperature without thermal activation in several hours and preserves the shape and the fluorescence of the building blocks. The assembled nanoparticle network provides longer exciton lifetimes with retained photoluminescence quantum yields, that make these nanostructured materials a perfect platform for novel multifunctional 3D networks in sensing. Various sets of photoelectrochemical measurements on the interconnected semiconductor nanorod structures also reveal the enhanced charge carrier separation.

can be achieved precisely, and the variety of appearance and functionality of the nanoparticles has extended the application possibilities of this material class in the fields of sensing,<sup>[2,3]</sup> energy harvesting,<sup>[4]</sup> (photo) catalysis,<sup>[5,6]</sup> photovoltaics,<sup>[7]</sup> and biomedicine.<sup>[8]</sup> Metal chalcogenides are excellent candidates for fulfilling the requirements of the above-mentioned fields of applications, due to the well-known quantum size effect emerging in their systems consisting of nanoscaled building blocks. This phenomenon endows these nanoparticle systems with unique and tunable optical properties.<sup>[9]</sup> The most widely used class of semiconductor nanoparticles is cadmium-chalcogenides, especially the CdSe/CdS and CdSe/CdTe heteroparticles in diverse size, shape, and functionality.<sup>[10]</sup> Most importantly, the high surface-to-volume ratio of nanocrystals further enhances the activity and applicability of them. Nevertheless, there are numerous fields, where liquid-based nanoparticle systems cannot be utilized, that has enhanced the development of different self-assembly procedures providing supported or non-supported superstructures.

## 1. Introduction

Control over the physical and physicochemical properties of semiconductor nanoparticles and their superstructures have become a cornerstone of the related research fields since the development of the modern synthesis methods of these novel nanoparticles.<sup>[1]</sup> Nowadays, fine-tuning of shape, size, surface chemistry, and optical properties of semiconductor nanocrystals

Two main objectives govern the preparation of these assemblies: i) the preservation of the individual nanocrystal properties and ii) the extension of these optical and physicochemical properties in the self-assembled nanosystems to pave the way toward new applications. In other words, novel nanoparticle-based superstructures should combine the properties of the building blocks and the emerging new features that can be

Dr. D. Zámbo, A. Schlosser, P. Rusch, F. Lübke, Prof. N. C. Bigall  
 Institute of Physical Chemistry and Electrochemistry  
 Leibniz Universität Hannover  
 Hannover 30167, Germany  
 E-mail: nadja.bigall@pci.uni-hannover.de

 The ORCID identification number(s) for the author(s) of this article can be found under <https://doi.org/10.1002/sml.201906934>.

© 2020 The Authors. Published by WILEY-VCH Verlag GmbH & Co. KGaA, Weinheim. This is an open access article under the terms of the Creative Commons Attribution-NonCommercial License, which permits use, distribution and reproduction in any medium, provided the original work is properly cited and is not used for commercial purposes.

DOI: 10.1002/sml.201906934

Dr. D. Zámbo, A. Schlosser, P. Rusch, F. Lübke, Prof. H. Pfnür,  
 Prof. N. C. Bigall  
 Laboratory of Nano and Quantum Engineering  
 Leibniz Universität Hannover  
 Hannover 30167, Germany

J. Koch, Prof. H. Pfnür  
 Institute of Solid State Physics  
 Leibniz Universität Hannover  
 Hannover 30167, Germany

Prof. N. C. Bigall  
 Cluster of Excellence PhoenixD (Photonics, Optics,  
 and Engineering – Innovation Across Disciplines)  
 Leibniz Universität Hannover  
 Hannover 30167, Germany

achieved solely based on the self-assembly of the nanocrystals. This challenging task has called numerous assembly procedures into being: triggering the responsive ligand shell,<sup>[11,12]</sup> cross-linking,<sup>[13,14]</sup> ligand desorption,<sup>[15]</sup> solvent exchange,<sup>[16]</sup> controlled solvent evaporation,<sup>[17]</sup> applying templates,<sup>[18]</sup> or using the cryoaerogelation method.<sup>[19,20]</sup>

Among the mentioned superstructures the monolithic, voluminous, and highly porous aerogels consisting of metal chalcogenide building blocks play a central role due to their advantageous feature: their non-supported nature. Since the development of nanoparticle-based aerogels,<sup>[21,22]</sup> a lot of effort has been made to extend the possibilities of nanoparticle (NP) aerogel formation.<sup>[23–29]</sup> We also demonstrated earlier, that interconnected macroscopic nanoparticle networks (voluminous aerogels) from dot-in-rod shaped nanoparticles<sup>[30]</sup> and core-crown nanoplatelets<sup>[31]</sup> can be achieved based on the partial oxidation of the surface ligands in aqueous medium. Notably, the dot-in-rod aerogels exhibit ultra-long exciton lifetimes besides high photoluminescence quantum yields. Nevertheless, oxidative methods are cumbersome to be applied for self-assembling oxygen-sensitive nanoparticles, such as, for example, CdTe, where significant quenching can be observed due to the oxidation of the nanocrystal (NC) surface.<sup>[32,33]</sup>

Triggering the self-assembly of cadmium chalcogenide nanocrystals in aqueous medium first requires the exchange of surface attached ligands generally from trioctylphosphine oxide (TOPO)/trioctylphosphine (TOP)/hexylphosphonic acid (HPA) to thiol-terminated carboxylic acids,<sup>[34]</sup> most commonly to 3-mercaptopropionic acid (MPA) or 11-mercaptopundecanoic acid (MUA). Employing a reliable phase-transfer method is of crucial importance in the preparation of colloiddally stable CdE (E = Se, S, Te) nanoparticles in water,<sup>[35,36]</sup> that extends the applicable agents to destabilize the nanoparticle solutions. Control over the destabilization process is the most important task in the preparation of porous, voluminous, macroscopic superstructures consisting of nanosized building blocks connected in a certain way. Thiolated or non-thiolated carboxylic acids, as capping agents, have been intensively studied recently in regard of metal ion sensing based on cadmium chalcogenide nanocrystals, due to the different affinity of metal cations to the carboxyl headgroup or to the surface of the nanocrystal itself.<sup>[3]</sup> Detection of, for example, calcium (II),<sup>[37]</sup> cobalt (II),<sup>[38]</sup> copper (II),<sup>[39]</sup> mercury (II),<sup>[40]</sup> or silver (I)<sup>[41]</sup> is based on the changes of optical properties of the nanocrystals upon addition of the cations (quenching, bleaching, or enhancement). The interaction between the cation and the surface of the nanocrystal or the ligand essentially governs the mechanism of the observed optical feature.<sup>[3]</sup> It is important to point out that the interaction of the cation and the nanoparticle surface might also induce the partial removal of the stabilizing ligands, that leads to the self-assembly of the nanoparticles. This phenomenon can be exploited efficiently for destabilizing the particles in a controlled manner: X-type capping ligands (such as thiolates, carboxylates, or phosphonates) can be suppressed/released from the NC surface by variety of Z-type ligands (e.g., metal halides like CdCl<sub>2</sub>, AlCl<sub>3</sub>).<sup>[42]</sup> This ligand exchange process has been demonstrated for instance by Lingley et al. from oleate to metal cation bound oleate on PbS nanocrystals,<sup>[43]</sup> and by Vanegas et al., who initiated the release of various thiolated ligands (2-mercaptoethanol, 7-mercapto-4-methylcoumarin, and MUA) from the surface of gold nanoparticles by means

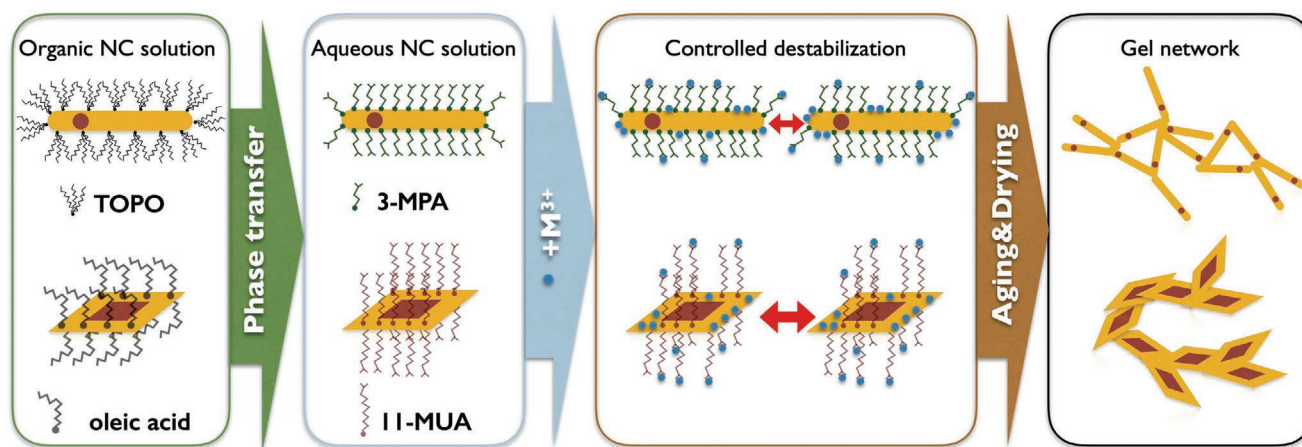
of lanthanide chlorides, that led to the aggregation of the particles.<sup>[44]</sup> In case of anisometric nanoparticles (nanorods, nanoplatelets), the ligand coverage is essentially influenced by the energies of crystal facets and the curvature of the nanocrystal. Consequently, the opportunity to direct the self-assembly of the nanoparticles is coded into the system through the controlled displacement of the ligands from the tip-region (nanorods, NRs) and edge-region (nanoplatelets, NPLs) of the building blocks.

In this paper, we demonstrate, that trivalent cations with high coordination numbers and charge densities can be used to induce the assembly of thiol-capped cadmium chalcogenide nanocrystals. The self-assembly results in the formation of interconnected, 3D nanoparticle network. The effect of concentration and nature of the added cations (Y<sup>3+</sup>, Yb<sup>3+</sup>, and Al<sup>3+</sup>) has been systematically investigated on a model system consisting of CdSe/CdS dot-in-rod shaped nanoparticles (45 nm × 4 nm in length and width, respectively) capped by MPA. Upon the assembly, interconnected nanorod-based gel networks have been prepared, whose structure was characterized by scanning electron microscopy (SEM) and transmission electron microscopy (TEM). The optical properties of the macroscopic assemblies (in form of solvogels and aerogels) prepared by different cations have been studied by means of UV-vis spectroscopy, spectrofluorometry, whereas the exciton lifetimes have been obtained by time-correlated single photon counting. The approach has been successfully extended to other cadmium chalcogenide nanoparticle heterostructure systems such as core/crown CdSe/CdS and CdSe/CdTe NPLs with different size, shape, and surface functionality. In each case, voluminous, photoluminescent, macroscopic 3D-assemblies have been prepared. To reveal the possible mechanism of the self-assembly, X-ray photoelectron spectroscopy (XPS) measurements have been performed and it has been demonstrated that the added cations have high affinity to the carboxyl groups as well as the NC surfaces and facilitate the crosslinking of the nanocrystals. Additionally, partial removal of the stabilizing surface ligands has also been observed, which also plays a role in the destabilization of the nanoparticle solutions. Due to the high concentration of the nanocrystal solutions, the assembly manifests itself in the formation of macroscopic gel-like structures, whose volume does not differ from the one of the initial NC solutions significantly. In addition, our method can be used to assemble nanoparticle systems sensitive to oxidation or elevated temperature. Besides TEM, the existence of the interconnected nanorod network has been supported by photoelectrochemical measurements, that are able to distinguish the charge carrier mobility processes in the assembled structures. The prolonged exciton lifetimes and charge carrier mobility show that these structures might be promising candidates for novel applications as photoelectrochemical sensors or photocatalysts. To the best of our knowledge, this is the first demonstration of the preparation of macroscopic semiconductor assemblies (e.g., aerogels) based on the destabilization of the aqueous colloidal solutions by means of trivalent cations.

## 2. Results and Discussion

### 2.1. Triggering the Self-Assembly via Trivalent Cations: the Structure of the Nanoparticle Gels

The TEM pictures of the as-synthesized nanoparticles can be seen in Figure S1, Supporting Information. The self-assembly



**Scheme 1.** Schematics of triggering the self-assembly of cadmium chalcogenide NRs (top row) and NPLs (bottom row) to prepare hyperbranched, 3D superstructures by addition of trivalent cations (represented as  $M^{3+}$ ).

process was deeply investigated and optimized on the model system of MPA-modified CdSe/CdS nanorods with the dimension of  $45 \text{ nm} \times 4 \text{ nm}$  (this nanoparticle model system is referred to as shorter NRs). **Scheme 1** demonstrates the process schematically on nanorods and nanoplatelets as well. After the addition of the  $Y^{3+}$  or  $Yb^{3+}$  salts, the aqueous nanorod solutions behaved differently according to the applied concentration (in the range of  $0.1$ – $10 \text{ mM}$ ). For  $0.1 \text{ mM}$ , no changes could be observed right after the mixing; however, more turbid and opalescent solutions formed with increasing cation concentrations. For  $5$  and  $10 \text{ mM}$ , the formation of the precipitates was visible by eye after several hours or tens of minutes, respectively. After  $17 \text{ h}$ , the volume of the fluffy precipitate varied as a function of the applied cation concentration: while in case of  $0.1 \text{ mM}$ , a colored supernatant and only a tiny precipitate at the bottom of the Eppendorf tube could be observed, the higher the cation concentration the higher the volume of the precipitate and more colorless supernatants appeared. It can be stated that for maximizing the volume of the assembled precipitate with the smallest volume of the colorless supernatant (namely the smallest contraction), addition of  $5 \text{ mM}$  of  $Y^{3+}$  or  $Yb^{3+}$  was found to be optimal. This concentration caused negligible (several volume%) contraction during the assembly, hence the volume of the initial nanorod solution can be preserved upon the self-assembly process. On the other hand,  $10 \text{ mM}$  cation caused only a slightly larger contraction; however, the formation of the initial gel structure was faster than for  $5 \text{ mM}$ . Hence, it was assumed that this might have a disadvantageous effect on the structure of the assembled network. At optimal conditions, the assembled system turned to a gel-like structure, that gives the basis of calling these precipitates “hydrogels.” The visual effect of the added cation concentration on the resulted assembled nanosystems can be seen in Figure S2, Supporting Information.

Due to the negligible volume of the precipitate and the significant amount of unassembled particles, it was not possible for hydrogels prepared via  $0.1 \text{ mM}$   $Y^{3+}$  and  $Yb^{3+}$  and  $1 \text{ mM}$   $Y^{3+}$  to be washed and transferred to acetone. For other concentrations, the shrinkage of the hydrogels was found to be negligible during washing and aging, which proves the formation of a

voluminous 3D nanoparticle assembly. Based on these findings, the assembly method was extended to other nanoparticle systems consisting of particles with different size, shape, composition, and surface ligand. Due to the experienced similarity between the effect of  $Y^{3+}$  and  $Yb^{3+}$ , these experiments were carried out using  $Y^{3+}$  salt. The assembly of longer nanorods and different nanoplatelets has also been optimized to obtain the largest volume of precipitate while keeping the shrinkage minimal. In case of longer, MPA-capped CdSe/CdS dot-in-rods (with a dimension of  $62 \text{ nm} \times 5 \text{ nm}$ , we refer to this system as “longer NRs” in the following) and MUA-capped CdSe/CdS and CdSe/CdTe nanoplatelets, the above described range of  $Y^{3+}$  concentration did not destabilize the systems appropriately; larger concentrations had to be applied to prepare hydrogels having the same appearance as that of shorter nanorods. For longer CdSe/CdS nanorods,  $15$ – $44.4 \text{ mM}$   $Y^{3+}$ , while for nanoplatelets,  $17 \text{ mM}$   $Y^{3+}$  was found to be suitable to prepare the 3D assembled nanostructures with the largest volume, least contraction and colorless supernatants. MUA-capped NPLs behave similarly to the MPA-capped NR systems, that underlines the versatility of the process from structural and surface chemical point of view. After the drying process, voluminous, lightweight, in certain cases monolithic aerogels from all the investigated nanoparticle systems were successfully obtained as depicted in **Figure 1**.

The effects of the cation concentration, the shape, and size of the nanoparticles on the structure of the aerogels were systematically investigated: **Figure 2** summarizes the electron microscopic images of the different model systems.

The self-assembled nanostructures have multimodal porosity and their voluminous nature originates from the mostly tip-to-tip connected nanorods and edge-to-edge connected nanoplatelets. **Figure 2** proves that the shape of the nanoparticles can be preserved during the assembly process, nevertheless, the building blocks are mostly fused, and the contact area is remarkable. This provides direct lattice contact between the nanoparticles (see **Figure S3**, Supporting Information, for more HR-TEM pictures) that enables an enhanced charge carrier separation through the three-dimensional network. The shape of the shorter nanorods could be completely preserved except for  $10 \text{ mM}$   $Y^{3+}$ , in this

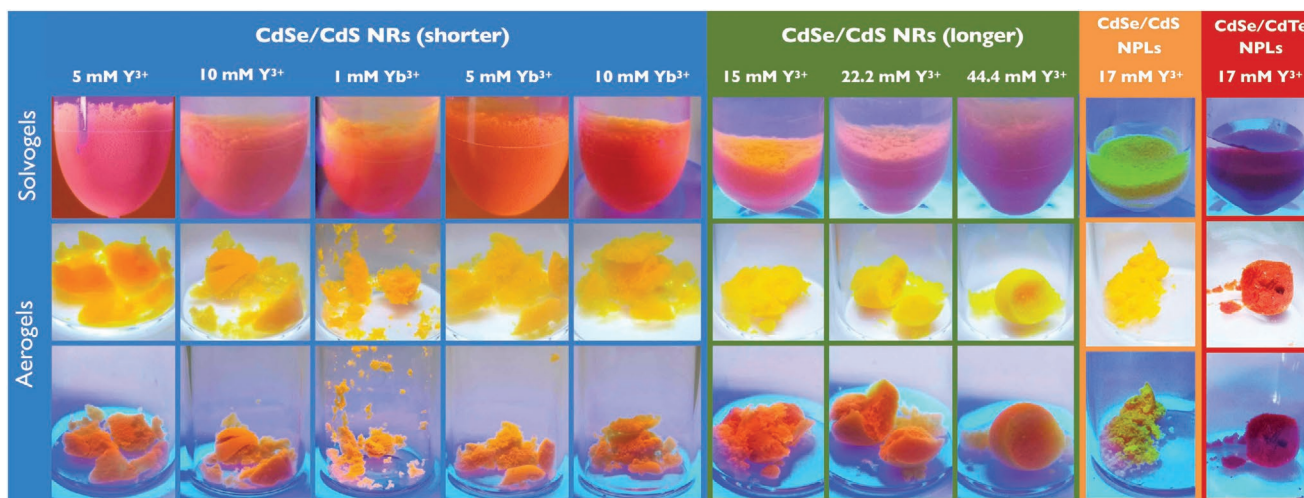


**Figure 1.** Photographs taken from solvogels (first row, in Eppendorf tubes) and aerogels (second and third rows) prepared from nanorods (CdSe/CdS) and nanoplatolets (CdSe/CdS and CdSe/CdTe) applying different  $Y^{3+}$  and  $Yb^{3+}$  concentrations and under different type of illumination (white LED and UV light for the second and third row, respectively).

particular case larger, spherical melted region were observed on the TEM images (see Figure S4, Supporting Information). In any other cases, regardless the size, shape, or surface ligands, the particles remained unchanged in the assembled network. It can be stated, that the final structure of the network already formed in the acetogels (anhydrous acetone as solvent) and remains similar after the drying process. **Figure 3** shows the structures of the acetogels prepared from nanorods and nanoplatolets. These images confirm, that the hyperbranched interconnected nanoparticle network already exists after the assembly in the form of solvogels, and the drying process does not have a significant influence on the structural behavior of the gels, however, changes in the optical properties can be observed. **Figure 4** shows the comparative HR-TEM images of the nanorod junctions in aerogels prepared from shorter (Figure 4a,b,d) and longer nanorods (Figure 4c) using trivalent cations and  $H_2O_2$  as gelation agents. It can be concluded, that using optimal concentration of  $H_2O_2$  (0.35%, based on our previous study)<sup>[30]</sup> resulted in more remarkable rod tips and smaller contact area between the rods. In contrast,  $Y^{3+}$  and  $Yb^{3+}$ -gelated nanorods are more fused and in crystal contact with larger contact area. This indicates a stronger and more direct particle-to-particle contact in the assembled network gelated via trivalent cations.

It has to be noted, that we also investigated the effect of  $Al^{3+}$  and it was found, that  $Al^{3+}$  can also trigger the assembly of the nanorods into similar gel networks as in case of  $Y^{3+}$  and  $Yb^{3+}$ . Upon addition of aluminum cations, very similar behavior and optical properties have been observed (see comparative SEM and TEM images in Figures S6 and S5, Supporting Information, for the optical properties), but the detailed investigation of the mechanism is not a part of the present study.

## 2.2. Optical Properties of Different Self-Assembled Structures

To reveal the changes in the optical properties during the self-assembly process, the absorption and PL spectra of different nanoparticles and assembled nanostructures have been

measured. The results show that the hydro- and aerogels preserved the characteristics of the absorption spectra of the nanocrystal solutions (for details see Figure S7, Supporting Information). The hydro- and aerogels are all photoluminescent, and the emission peak of the aerogel samples shifted bathochromically (up to 25 nm), that can be attributed to the complex effect of refractive index change upon drying as well as of the nanoparticle network formation with direct interparticle contacts.

Fluorescence lifetime measurements (time-correlated single photon counting) were also carried out on the pristine building blocks as well as assembled structures. The fluorescence lifetime decays change dramatically due to the formation of the network-like, assembled aerogel structures for all concentrations of the applied cations. The slope of the decay curves decreases with increasing  $Y^{3+}$  and  $Yb^{3+}$  concentrations, especially for longer nanorods, where a higher concentration of the destabilizing agent is required, therefore the decay of the aerogels of longer rods does not differ from the one of the free rods drastically. The most prominent change can be observed for 1 mM of  $Yb^{3+}$  (Figure S8c, Supporting Information): the largest contribution of  $\tau_2$  and the longest average exciton lifetime (41.3 ns) can be achieved (Table S1, Supporting Information, contains the fitting parameters of the PL decay curves and the average PL lifetimes for each sample). It can be concluded, that the self-assembly process manifests itself in longer exciton lifetimes for all model systems and the lifetime of the aerogels are higher at lower concentrations of the cations (for further discussion of the optics, please refer to the Supporting Information). These observations agree well with our recently published results, where both of our experimental studies and theoretical calculations showed the possibility of enhanced electron-hole separation in coupled CdSe/CdS dot-in-rod systems, while no delocalization was observed for decoupled building blocks (nanorods covered by silica shell before the assembly).<sup>[45]</sup> In addition, the resulting enhanced charge carrier mobility can be utilized in photoelectrochemical reactions (discussed later in the paper).

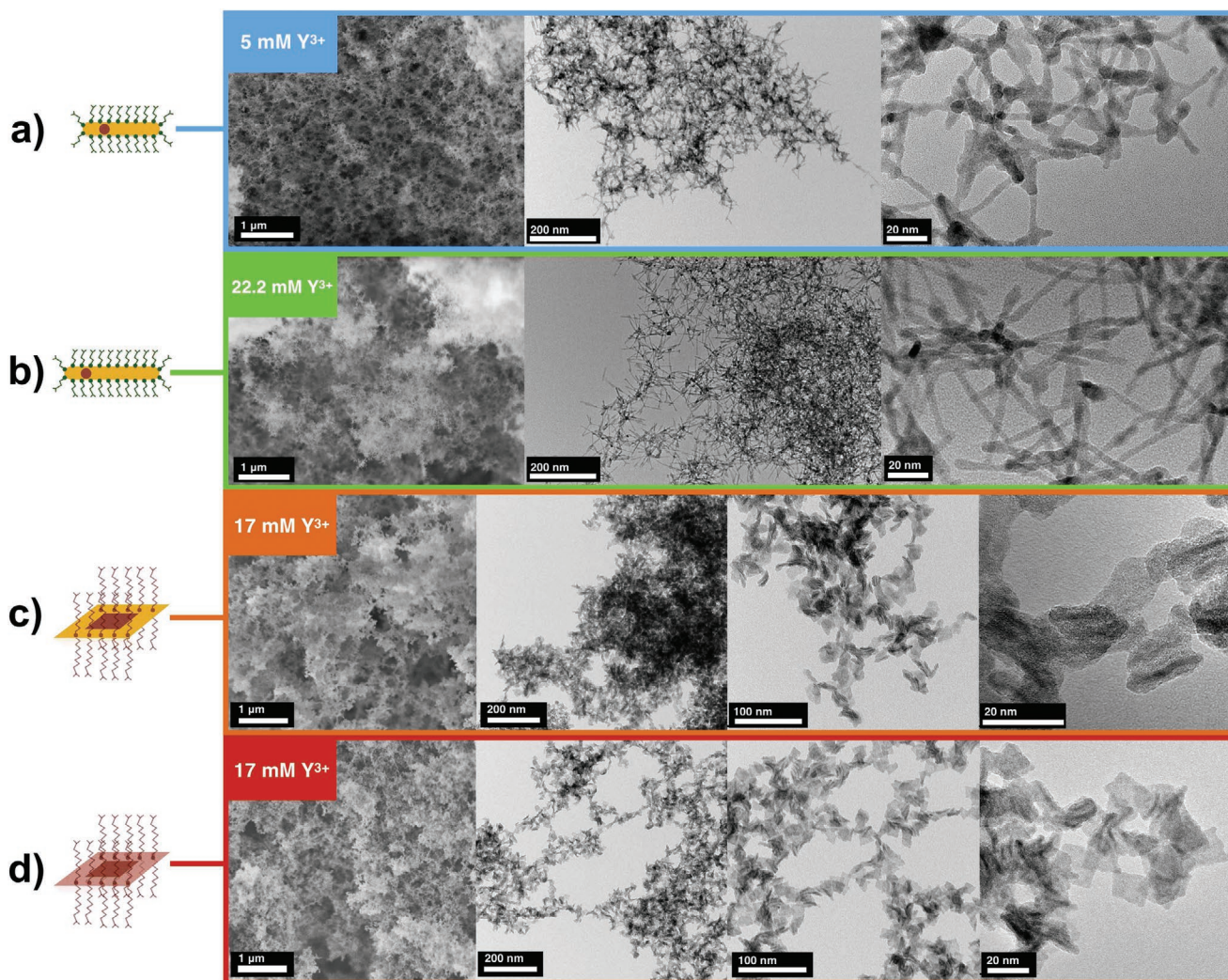


**Figure 2.** Structural characterization (SEM and TEM images) of aerogels prepared using different concentration of  $Y^{3+}$  salt. Blue rectangle represents the structure of aerogels built up from shorter ( $45 \times 4$  nm) nanorods (a), while green rectangle shows the structures from longer ( $62 \text{ nm} \times 5$  nm) nanorods (b). Aerogel structures obtained from CdSe/CdS and CdSe/CdTe NPLs are represented with orange (c) and red (d) rectangles, respectively.

Based on the results of structural and optical investigations, the optimal concentration of  $Y^{3+}$  and  $Yb^{3+}$  was found to be 5 mM for shorter nanorods and 22.2 mM for longer ones. This allowed to preserve the shape of the nanorods, to ensure the washing and handling of the gels and to prepare tip-to-tip connected particle network with enhanced exciton lifetimes and enhanced QYs (see Figure S10, Supporting Information, for details).

For CdSe/CdS nanoplatelets, no prominent changes can be observed in the PL decays (see Figure S9a, Supporting Information); the average exciton lifetime increases from 6.8 to 13.0 ns. This is in good agreement with our recent results on  $H_2O_2$  triggered self-assembly of CdSe/CdS nanoplatelets.<sup>[31]</sup> However, in case of CdSe/CdTe nanoplatelets, the self-assembly leads to extended exciton lifetimes (up to 40.8 ns) in form of hydro- and aerogel as well (Figure S9b, Supporting Information). This result shows that the charge carrier separation can be achieved in the assembled structure consisting of CdSe/CdTe core-crown nanoplatelets as well. It is known that CdTe is extremely sensitive to oxidation, that made our effort cumbersome toward the formation

of solvo- and aerogels based on the ligand oxidation methods beforehand (applying, e.g.,  $H_2O_2$  or hydrazine as destabilizing agents). The quantum yield of the aerogels prepared by the above-mentioned oxidative methods decreased to zero and led to the complete etching of the CdTe crown at higher gelation agent concentrations (at lower concentrations the gelation did not take place). However, based on the TEM images of the  $Y^{3+}$ -triggered self-assembled NPL structures, the CdTe crown region remained intact during the formation of the 3D network. The measured QYs of the hydrogels and aerogels of CdSe/CdTe NPLs supports this statement as well: the QY of the aqueous nanoplatelet solution can be retained after the aerogel formation just like in case of shorter and longer nanorods (Figure S10c, Supporting Information).

### 2.3. Control Experiments

In order to rule out the salting-out effect caused by the increased ionic strengths in the nanoparticle solutions, control

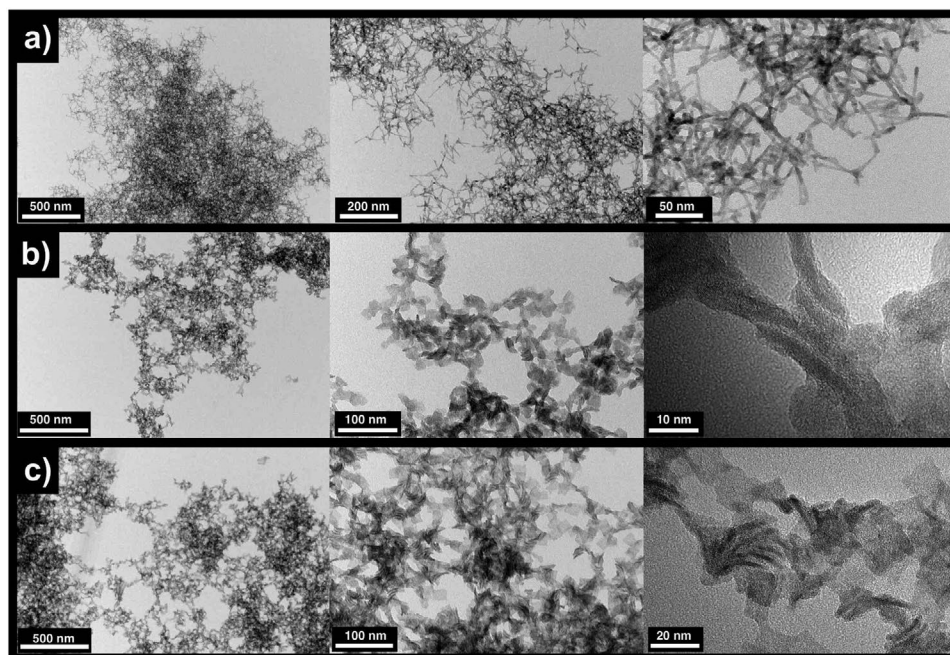


**Figure 3.** TEM images in different magnifications of solvogels prepared from shorter CdSe/CdS nanorods treated with 5 mM  $\text{Yb}^{3+}$  (a), CdSe/CdS NPLs (b) and CdSe/CdTe NPLs (c) treated with 17 mM  $\text{Y}^{3+}$ .

experiments with added NaCl solution have been carried out. The concentration of the NaCl has been calculated to set the same ionic strengths as in case of 5 and 10 mM  $\text{YCl}_3$  and  $\text{YbCl}_3$  for shorter nanorods (this corresponds to 30 and 60 mM of NaCl, respectively). The changes in the size distribution of the nanorod solutions were monitored via dynamic light scattering. As Figure S11, Supporting Information, demonstrates, the size of the nanoparticles does not change at all in the observed time

range (24 h) after the addition of the NaCl solutions. No precipitation and sedimentation can be observed in the nanoparticle solutions containing NaCl either after 5 months of the addition. Salting out effect can be initiated solely at much higher NaCl concentrations (above 300 mM), where the particles sediment and form a much more shrunken precipitate, that is a drastic difference compared to the case of the  $\text{Y}^{3+}$  or  $\text{Yb}^{3+}$ -initiated assembly. These experiments demonstrate the different

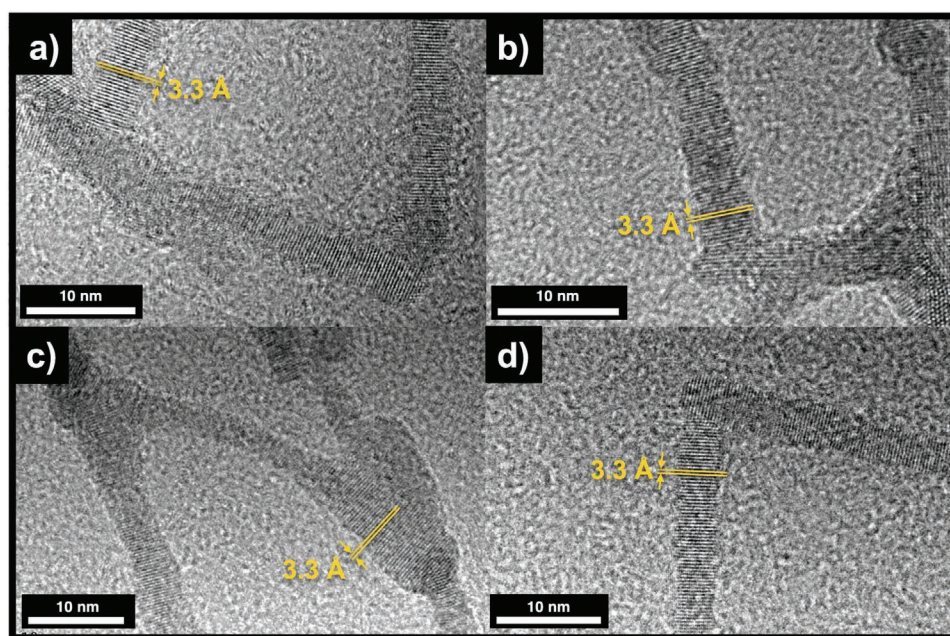


**Figure 4.** HR-TEM images of the nanoparticle junctions in aerogels prepared from shorter CdSe/CdS nanorods treated with 5 mM  $\text{Y}^{3+}$  (a) and 5 mM  $\text{Yb}^{3+}$  (b), longer CdSe/CdS nanorods treated with 22.2 mM  $\text{Y}^{3+}$  (c). As a comparison, panel (d) shows shorter rods assembled via 0.35%  $\text{H}_2\text{O}_2$ .

mechanism of the assembly and the difference between salted-out systems and gelled ones.

#### 2.4. Effect of Trivalent Cations on the Self-Assembly

During the aerogel formation, numerous washing steps with different solvents are carried out on the self-assembled nanoparticle networks. These washing steps are of importance in the aspect of aging and removal of the excess of the cation and unbound ligands.<sup>[30]</sup> As it is detailed in the experimental section, the hydrogels have been washed with MilliQ water, water-acetone mixtures, dry acetone, and finally with liquid CO<sub>2</sub> to change the medium of the gel from liquid to air. In spite of all these thorough washing steps, EDXS analysis shows that the aerogels contain significant amounts of Y<sup>3+</sup> and Yb<sup>3+</sup> (Figure S12, Supporting Information, shows the detailed quantitative elemental analysis on the NR and NPL aerogel samples). Hence, it can be anticipated, that the interaction between the cations (III) and the surface of the nanoparticles or the ligands is significant. It has to be noted that the amount of chlorine was found to be negligible in the majority of the samples, which shows, that the cation is not present in the form of the initial salt (namely YCl<sub>3</sub> and YbCl<sub>3</sub> crystals) more likely in the form of surface attached or coordinated cations. This statement is also supported by the fact that salt crystals were never found in the solvogel or aerogel samples investigated by SEM or TEM. Due to the existence of Yb<sup>3+</sup> in the aerogel samples, the PL spectra of aerogels containing 1 and 10 mM Yb<sup>3+</sup> were measured in the NIR wavelength range as well. It is known that Yb<sup>3+</sup> has a strong luminescence in the range of 950–1100 nm with two prominent peaks around 980 and 1019 nm,<sup>[46]</sup> thus the question appeared, whether the surface attached Yb<sup>3+</sup> has still a luminescence in the aerogel samples. However, the sign of the Yb<sup>3+</sup> luminescence features could not be found in the samples containing Yb<sup>3+</sup>, not even at 10 mM Yb<sup>3+</sup> concentration (see Figure S13, Supporting Information, for the PL spectra). These results point out that the lanthanide's luminescence is totally quenched due to the presence of coordinated atoms/chemical groups or the vicinity of the nanoparticle surface.

To reveal the governing interactions between the cations and surface/ligands of the nanoparticles, XPS analysis has been performed on the shorter CdSe/CdS nanorod model system. Figure 5 shows the XPS spectra of the precipitates (containing the nanoparticles in the form of individual NRs (for reference, without added cations) and in the form of interconnected network (formed after the addition of the cations) and the supernatants (clear aqueous phase without NRs) in the binding energy range of S 2s, S 2p, and O 1s. The binding energies of the relevant elements can be found in Table S2, Supporting Information. Four main statements can be phrased based on the XPS results: i) the amount of sulfur species (especially S–H bonds) increases in the supernatant dramatically after the addition of both of the cations, ii) the amount of sulfur species increases in the precipitates after the gel formation and the peaks are shifted toward the higher binding energies, which can be attributed to the S–S and S–C bonds in the partially released ligands trapped in the porous NR structure, iii) a new peak evolves at lower binding energies in the O 1s

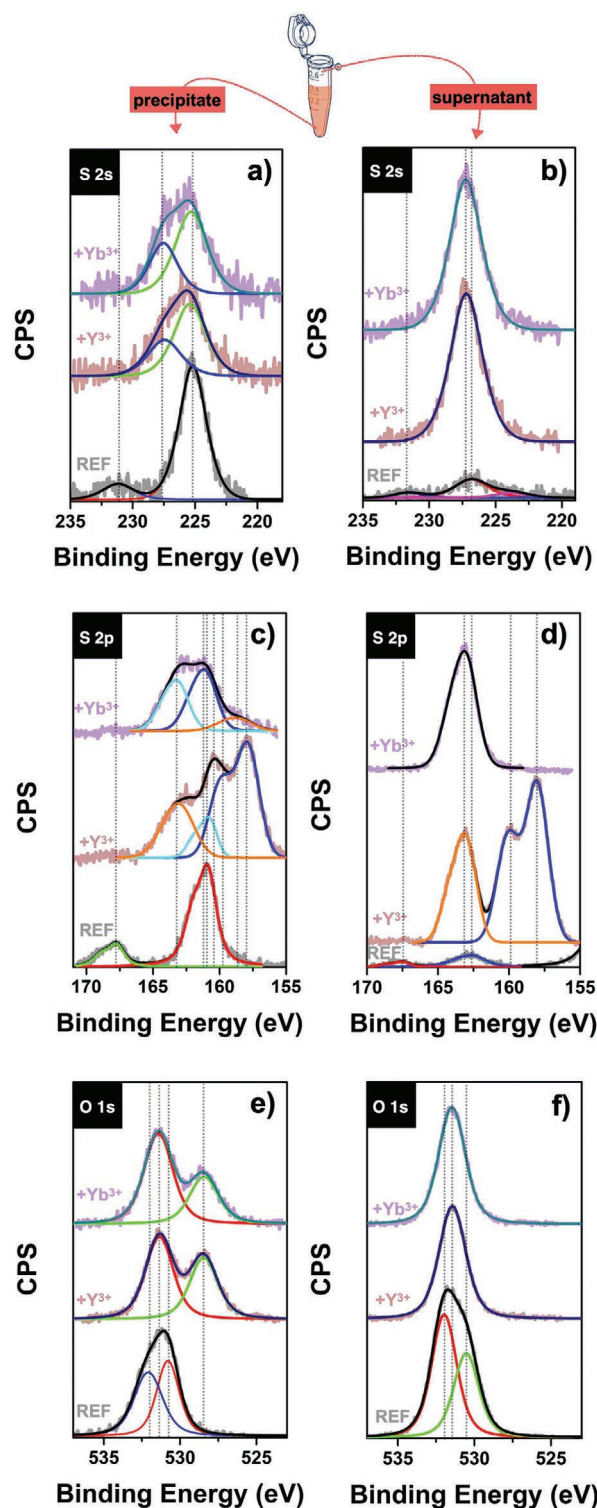


**Figure 5.** XPS spectra in the binding energy range of S 2s (a,b), S 2p (c,d) and O 1s (e,f) for precipitates (a,c,e) and supernatants (b,d,f). Each spectrum contains the reference (no Y<sup>3+</sup> or Yb<sup>3+</sup> added, only the pure CdSe/CdS@MPA rods), the samples containing 10 mM Y<sup>3+</sup> and 10 mM Yb<sup>3+</sup>. The dashed lines correspond to the peak positions to help the comparison as guides to the eye. Note, that in case of +Y<sup>3+</sup> samples in panel (c) and (d), Y 3d peaks (in the range of 158–160 eV, blue fitted curves) are overlapping with the low energy S 2p peak.

precipitate spectra after the addition of the cations, that can be explained by the coordination of the cation with the carbonyl group of the surface attached MPA, iv) cadmium cannot be found in the supernatants neither in the case of the reference samples nor of the samples after addition of the cations (see Figure S14, Supporting Information, for the Cd 3p and Cd 3d XPS spectra). These results suggest that two processes are present at the same time after the addition of the cations. First, the cations coordinate in the vicinity of the surface attached MPA carboxyl groups and facilitate the crosslinking of the nanoparticles. Second, the cations attach to the surface of the CdS shell of the nanorods and partially replace the surface grafted ligands, that manifests itself in the increasing amount of sulfur species in the supernatants (the released ligands diffuse to the aqueous medium of the gel, which can be collected from the supernatants after centrifugation). Although the cations might reduce the Debye length of the electrostatically charged nanoparticles, the self-assembly cannot be explained based on solely screening effects in the applied ionic strength range as the control experiments show (applying NaCl instead of  $YCl_3$  or  $YbCl_3$ ). These findings are in good agreement with the revealed effect of the lanthanides on the surface of gold nanoparticles modified by MPA and MUA<sup>[44,47]</sup> and emphasize the importance of the ligand replacements process in the framework of our self-assembly experiments.

## 2.5. Photoelectrochemical Measurements

To characterize the transport of charge carriers across the CdSe/CdS nanorod network structures, linear sweep voltammetry (LSV) and intensity modulated photocurrent spectroscopy (IMPS) were applied. Therefore, photoelectrodes coated with CdSe/CdS nanorod based xerogels were prepared by drying the respective hydrogels under ambient conditions (see the details in the experimental section in the Supporting Information). All measurements were performed in a sodium sulfite buffer solution (pH 9) under periodic irradiation by a light emitting diode (LED) light source ( $\lambda_{max} = 472, 523, \text{ or } 600 \text{ nm}$ ). The LSVs of the shorter CdSe/CdS nanorod xerogel after different electrolyte exposure times are displayed in Figure 6a.

The measured photocurrent was observed to increase with increasing electrolyte exposure time in the whole bias potential range. This observation could be related to the continuous hydration of the densely packed xerogel structure, which leads to an increase in the contact area between the particles and the electrolyte.<sup>[48]</sup> Nearly stable photocurrents of up to  $6 \mu\text{A cm}^{-2}$  were obtained after 23 h of electrolyte exposure and very low dark currents were recorded throughout all measurements. Furthermore, only positive photocurrents were registered in the whole investigated time and potential range. In the applied electrolyte, positive photocurrents originate from the following two processes: i) oxidation of sulfite to sulfate by hole extraction from the semiconductor nanoparticle and ii) electron injection into the electrode.<sup>[49]</sup> Consequently, the hole extraction from the CdSe cores seems to be much faster and/or more effective than the electron extraction from the shell (which would lead to negative photocurrents). This result is in line with the fluorescence lifetime measurements, which already revealed, that excited

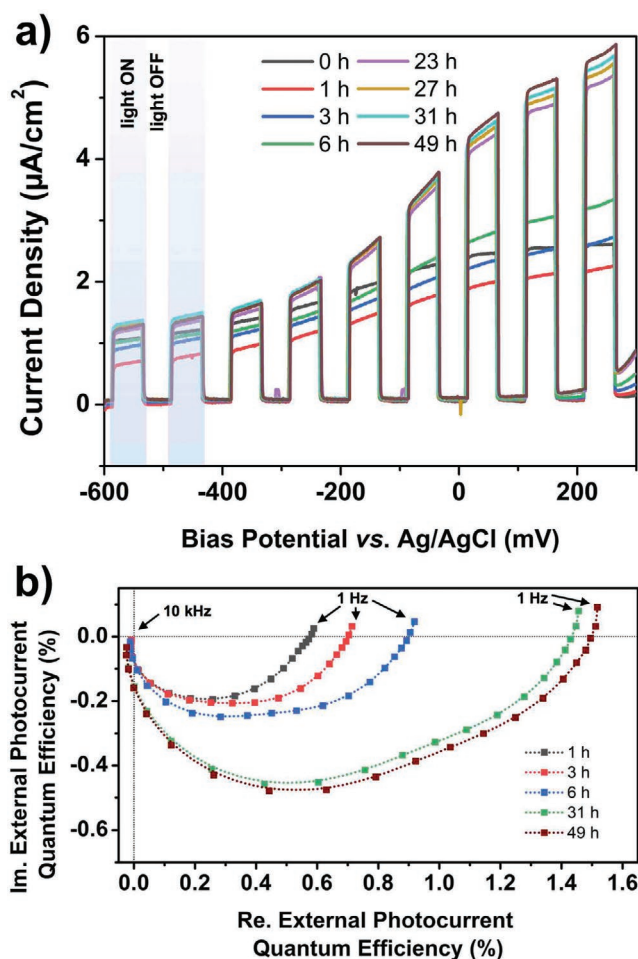


**Figure 6.** Linear sweep voltammograms (a) and Nyquist complex plane plots (obtained from intensity modulated photocurrent spectra (IMPS)) (b) on shorter CdSe/CdS NRs + 5 mM  $Y^{3+}$ . The blue shaded parts represent the periods, where the LED light source ( $\lambda = 472 \text{ nm}$ ) was turned on. The dotted lines on panel (b) are guide to the eye.

electrons are delocalized and can therefore move across the CdSe/CdS nanorod network whereas the holes remain in the CdSe cores. A similar behavior (only positive photocurrents) was previously reported for inkjet-printed CdSe/CdS nanorod based xerogel films, with the difference, that in the first hours after electrolyte exposure also negative photocurrents at low bias potentials were observed.<sup>[48,50]</sup> The occurrence of a photoelectrochemical photocurrent switching (PEPS) point in the LSVs is typical for CdSe/CdS nanorod monolayers,<sup>[48,51]</sup> so that in our case the re-hydration of the xerogel structure seems to proceed much faster than in case of the inkjet-printed nanorod xerogels. The re-hydration of the gel structure as well as charge carrier transport across the nanorod network in general was furthermore investigated by means of IMPS. Regardless of the electrolyte exposure time, two overlapping semicircles were observed in the IMPS responses of the xerogel (Figure 6b). The high frequency semicircles correspond in all cases to charge carrier transfer processes involving particles located directly at the ITO surface whereas the lower frequency semicircles can be attributed to the diffusion of charge carriers generated further

away from the electrode surface. From the IMPS responses, an increasing contribution of the latter processes to the photocurrent with increasing electrolyte exposure time (advancing re-hydration) can be deduced, as the diameter of low frequency semicircle was observed to increase much faster than the diameter of the high frequency semicircle (more detailed discussion of the results and additional photoelectrochemical measurements can be found in the Supporting Information).

The results of the photoelectrochemical measurements revealed that electrons are able to move across the nanoparticle network, which supports the statements made based on the spectroscopic results. It was found that the photoelectrochemical response and the re-hydration of the fabricated electrodes are fast (occurs in less than 24 h), that makes them a potential candidate for applying them as quick photoelectrochemical sensors. In addition, no remarkable influences of the nature of the trivalent cation or the nanorod size on the charge carrier transport were observed.

### 3. Conclusion

A novel way to prepare photoluminescent voluminous aerogels consisting of interconnected semiconductor nanoparticles has been demonstrated. The self-assembly has been initiated by the addition of trivalent cations ( $Y^{3+}$  and  $Yb^{3+}$ ) to the aqueous solutions of different nanoparticles: MPA-capped CdSe/CdS dot-in-rod shaped nanoparticles and MUA-capped CdSe/CdS as well as CdSe/CdTe core/crown nanoplatelets. Under optimized conditions, three-dimensional assemblies consisting of tip-to-tip connected nanorods and edge-to-edge connected nanoplatelets with lattice contacts can be obtained. This nanostructural feature enables the enhancement of the charge carrier separation throughout the hyperbranched network, that leads to longer exciton lifetimes and higher photoluminescence quantum yields compared to the aqueous solutions of individual nanoparticles. Based on the XPS measurements it can be concluded that the added cations bind strongly to the surface of the nanoparticles facilitating the partial removal of the ligands from the nanoparticle surface. The applied assembly method has numerous key advantages: i) due to its non-oxidative nature, the method can be applied to assemble oxidation-sensitive nanoparticles; ii) it does not require thermal activation, the assembly takes place at room temperature; iii) its versatility enables the formation of 3D nanoparticle networks from building blocks possessing different chemical composition, surface ligands or shapes. Photoelectrodes (3D assemblies on ITO covered glass) have been successfully prepared and the interconnection of the nanorods in the network has also been proven by linear sweep voltammetry and intensity modulated photocurrent spectroscopy. It was found that the structures can be hydrated fast, which paves the way toward possible future applications of these 3D superstructures as fast photoelectrochemical sensors.

### 4. Experimental Section

**Reagents and Materials:** Cadmium oxide (CdO, 99.998%), cadmium nitrate tetrahydrate ( $Cd(NO_3)_2 \cdot 4H_2O$ , 99.999 %), elemental selenium

(200 mesh, 99.999%), and oleic acid (OLA, > 90%) were supplied by Alfa Aesar. Sodium myristate (Na(myristate), > 99%), tri-*n*-octylphosphine oxide (TOPO, 99%), elemental sulfur (99.98%), 1-octadecene (ODE, 90%), 3-mercaptopropionic acid (MPA, ≥99%), 11-mercaptoundecanoic acid (MUA, 95%), ammonium hydroxide ( $NH_4OH$ , 28–30 wt%), (3-mercaptopropyl)trimethoxy-silane (MPTMS, 95%), sulfuric acid ( $H_2SO_4$ , 95–97%), 2-propanol (≥99.8%), chloroform (≥99.5%), yttrium chloride hexahydrate ( $YCl_3 \cdot 6H_2O$ , 99.99%), and ytterbium chloride hexahydrate ( $YbCl_3 \cdot 6H_2O$ , 99.9%) were purchased from Sigma-Aldrich. Potassium hydroxide (KOH, >85%), *n*-hexane (≥99%), acetone (99.5%), hydrogen peroxide ( $H_2O_2$ , 35 w/w%), toluene (≥99.7%), and methanol (MeOH, ≥99.8%) were purchased from Honeywell. Ethanol (EtOH, ≥99.8%), sodium sulfite ( $Na_2SO_3$ , >97%), tri-*n*-octylphosphine (TOP, 97%), elemental tellurium (60 mesh, 99.999%), cadmium acetate dihydrate ( $Cd(OAc)_2 \cdot 2H_2O$ , >98%), octadecylphosphonic acid (ODPA, 99.0%), and hexylphosphonic acid (HPA, 99%) were obtained from Roth, Fisher Scientific, ABCR and PCI, respectively. All chemicals were used as received without further purification. For aqueous solutions, ultrapure water with a resistivity of 18.2 MΩ-cm was used in all cases.

**Synthesis of CdSe Quantum Dots:** The synthesis of CdSe quantum dots has been carried out following the protocol published elsewhere.<sup>[17]</sup> First, 0.116 g of elemental selenium was dissolved in 3.6 mL TOP under vigorous stirring at 40 °C for 24 h in a glove box. CdO (0.12 g), TOPO (6.0 g), and ODPA (0.56 g) were mixed in a three-neck flask and degassed under vacuum and stirring at 150 °C for 1 h in a Schlenk-line system. Subsequently, the atmosphere was changed to argon and the temperature was brought to 300 °C until the CdO dissolved completely. TOP (3.6 mL) was injected into the reaction mixture and the temperature was increased to 380 °C. When the temperature reached the value of 380 °C, the previously prepared TOP:Se solution (3.6 mL) was injected rapidly. The reaction was allowed to proceed for 4 min following the injection of 6 mL ODE to stop the growing of the nanocrystals and the system started to be cooled down to room temperature by removing the heating mantle. At 80 °C, 5 mL of toluene was added to the solution to avoid the recrystallization of the solvent. When the system reached the room temperature, the QD solution was transferred to a Falcon tube, 10 mL of MeOH was added to precipitate the particles and centrifuged (10.000 g, 5 min). The clear supernatant was discarded and the QDs were redispersed in toluene. The cleaning process was repeated once more and the QDs were redispersed in low volume of toluene (≈1.5 mL). The concentration and the size of the QDs in this final solution were determined based on the absorption spectrum.<sup>[52]</sup> The diameter of the QDs and the concentration of the toluene solution were found to be 3.4 nm and 1.549 mm, respectively.

**Synthesis of CdSe/CdS Dot-in-Rod Nanoparticles:** The growth of the CdS around the CdSe core QDs to obtain dot-in-rod-like nanoparticles was carried out using an upscaled and slightly modified synthesis procedure of Sánchez-Paradinas et al.<sup>[30]</sup> First, the TOP:S solution was prepared in a glove box by dissolving of elemental sulfur (0.383 g) in TOP (5.5 mL) under vigorous stirring at 40 °C for 24 h. For obtaining shorter NRs, CdO (0.18 g), HPA (0.24 g), ODPA (0.84 g), and TOPO (9.0 g) were mixed in a three-neck flask and degassed under vacuum for 1 h at 150 °C. After changing the atmosphere to argon, the temperature was raised to 300 °C and TOP (5.5 mL) was injected instantaneously. Right after the injection, the temperature was set to 380 °C and kept until the complete dissolution of the precursor (≈0.5–1 h). A calculated volume of the concentrated toluene solution of the CdSe QDs was mixed with the previously prepared TOP:S solution (5.5 mL) ensuring the final concentration of the cores in the total growing solution to be 400 μM. This CdSe:TOP:S mixture was injected rapidly into the solution with a syringe and the reaction was allowed to proceed for 8 min, after which the system was cooled down to room temperature. At 80 °C, toluene (10 mL) was added to the solution and after reaching RT, the particles were precipitated by MeOH (10 mL) and centrifuged (3700 g, 10 min). The nanorods were washed with centrifuging/redispersion (toluene) cycles at least three times to remove the excess of stabilizer and unreacted precursor. Finally, the NRs were redispersed and stored in 6 mL of toluene. For preparing longer nanorods, 0.27 g CdO was used

instead of 0.18 g. Based on the TEM images, the length and the width of the shorter NRs were found to be 45 and 4 nm respectively, while for longer rods, these values were 62 and 5 nm.

**Synthesis of Cadmium Myristate and Cadmium Propionate:** Cadmium myristate and cadmium propionate were synthesized according to previously published protocols.<sup>[53,54]</sup>

**Synthesis of CdSe Core Nanoplatelets:** CdSe core nanoplatelets with a thickness of four monolayers (MLs) were synthesized following a slightly modified literature procedure.<sup>[55]</sup> Briefly, cadmium myristate (2.4 mmol, 1.36 g) and selenium powder (1.4 mmol, 0.108 g) were dispersed in ODE (120 mL) in a 250 mL three necked round bottom flask. The mixture was degassed at 70 °C twice for 30 min and subsequently heated to 240 °C under an Ar atmosphere. At a temperature of 205 °C, solid cadmium acetate dihydrate (2.4 mmol, 0.640 g) was swiftly added to the orange solution. The reaction was allowed to proceed for 8 min at 240 °C and was then quenched by the addition of oleic acid (8 mL). When the red solution was cooled down to room temperature, 50 mL of ethanol was added, and the mixture was centrifuged for 10 min at 4226 g. The red supernatant was discarded while the yellow precipitates were dissolved in 60 mL of hexane and centrifuged for 10 min at 4226 g. To the supernatant, which solely contained the desired 4 ML NPLs, ethanol (20 mL) was added. The product was collected by centrifugation (10 min, 4226 g) and was redispersed in hexane (10 mL). Based on the TEM images, the core NPLs have a dimension of 14 × 11 nm.

**Synthesis of CdSe/CdS Core/Crown Nanoplatelets:** For the growth of CdS crowns around the CdSe NPL edges, a procedure by Tessier et al.<sup>[53]</sup> was applied with slight modifications. At first, CdSe NPL solution in hexane (2.25 mL, Cd concentration: 42.9 mM) was mixed with ODE (5 mL) in a 25 mL three necked round bottom flask. The hexane was removed by degassing the solution twice for 30 min at 80 °C. Subsequently, the solution was heated to 240 °C under an Ar atmosphere, and a growth solution containing cadmium and sulfur precursors was injected at a rate of 12 mL h<sup>-1</sup> for 15 min. The growth solution was prepared beforehand by heating a mixture composed of cadmium acetate dihydrate (1.8 mmol, 0.48 g), oleic acid (1.1 mmol, 0.340 mL), and ODE (2 mL) to 120 °C for 30 min and mixing the resulting greyish gel with S/ODE (3 mL, 0.1 M) suspension. After completion of the injection, the reaction solution was quickly cooled down to room temperature and hexane/ethanol (10 mL, 1:1) mixture were added. The solution was then centrifuged at 4226 g for 10 min and the CdSe/CdS NPLs were redispersed in hexane (2 mL). Based on the TEM images, the NPLs have a dimension of 26 nm × 15 nm.

**Synthesis of CdSe/CdTe Core-Crown Nanoplatelets:** CdSe/CdTe core/crown nanoplatelets were synthesized following the procedure by Pedetti et al.<sup>[56]</sup> In a 25 mL three necked round bottom flask, CdSe NPL solution in hexane (2.25 mL, Cd concentration: 42.9 mM), cadmium propionate (1.0 mmol, 0.26 g), and oleic acid (1.5 mmol, 0.476 mL) were dissolved in ODE (10 mL). The mixture was degassed in vacuum twice (80 °C, 30 min) to remove the hexane and dissolved gases. Afterward, the reaction solution was heated to 235 °C and a solution of TOP:Te (1 M, 0.1 mL) dissolved in ODE (2 mL) was injected at a rate of 48 mL h<sup>-1</sup>. The reaction solution was kept at 235 °C for 15 min and was then cooled down to room temperature. Subsequently, hexane (5 mL) and ethanol (7.5 mL) were added, and the mixture was centrifuged for 10 min at 4226 g. Finally, the CdSe/CdTe NPLs were redispersed in hexane (2 mL). Based on the TEM images, the NPLs have a dimension of 23 nm × 18 nm.

**Water Transfer of Semiconductor Nanoparticles:** The transfer of semiconductor nanoparticles from organic solution to aqueous media was carried out following the procedure published by Kodanek et al.<sup>[36]</sup> For CdSe/CdS dot-in-rods, the nanoparticles (6 mL in toluene) were precipitated by adding MeOH, centrifuged, and redispersed in hexane (6 mL). Transfer solution (consisting of 15 mL MeOH, 0.32 g KOH, and 0.388 mL 3-MPA) was added and the mixture and was shaken on an orbital shaker overnight. The two phases were allowed to be separated and the colored aqueous phase was removed and centrifuged. The particles were redispersed in KOH solution (0.1 M, 6 mL). In order to remove all organic residue, chloroform (1.5 mL) was added, and

the solution was vortexed and centrifuged. Finally, the particles were redispersed in aqueous KOH solution (0.1 M, 6 mL) forming a water clear orange/reddish solution. The Cd-concentration of the solution was determined by AAS (after dissolving the nanoparticles in aqua regia) and was set to the value of 3.6 g L<sup>-1</sup> in the final, aqueous nanoparticle solution by diluting them with Millipore water (the final concentration of the KOH was 0.02 M). The water-transfer of NPLs differed slightly: CdSe/CdX (X = S, Te) NPL solution in hexane (1.8 mL, Cd concentration: 20 mM) were mixed with a solution consisting of MUA (0.16 mmol, 0.0348 g) and KOH (0.36 mmol, 0.0205 g) dissolved in methanol (2.5 mL). The mixture was shaken overnight in the dark. Afterward, the colorless hexane phase was removed and the remaining solution containing the NPLs was centrifuged at 4226 g for 10 min. The precipitate was then redispersed in aqueous KOH (0.1 M, 1 mL) and washed with acetone (1 mL) and 2-propanol (1 mL), respectively. Finally, the purified NPLs were redispersed in aqueous KOH (0.1 M, 1 mL).

**Destabilizing the Nanoparticles: Preparation of Hydrogels and Acetogels:** Self-assembly of the nanoparticles was triggered by use of aqueous solution of YCl<sub>3</sub>·6H<sub>2</sub>O and YbCl<sub>3</sub>·6H<sub>2</sub>O salts in varied concentrations. 50 µL salt solution was injected into the 400 µL aqueous solution of semiconductor nanoparticles ( $c_{Cd} = 3.6 \text{ g L}^{-1}$ ) in an Eppendorf tube followed by a rapid vortexing. The solutions were stored at room temperature for 17 h in a dark place free from vibrations. Thereafter, the clear, small volume of supernatant (if appeared) was removed and the spongy, fluffy assembled precipitate was washed gently with MilliQ water in 1–1.5 mL portions. This washing step was carried out slowly, meaning that the process contained nine steps (addition and removal of MilliQ) and lasted ≈3–4 h. The last step was done 24 h later to ensure, that all of the remaining salt was removed completely. Subsequently, the medium of the precipitate was gradually changed from water to acetone through water:acetone mixtures (from 10:1 to 1:5 as water:acetone volume ratio) in slow steps during 2 days. Finally, the medium was changed to anhydrous acetone by washing the system with dry acetone consecutively in 5 days. During this period, the so-called “aging” of the self-assembled superstructure also takes place and the compatibility with the supercritical drying has also been ensured.

**Preparation of Aerogels:** The completely washed acetogels (in anhydrous acetone) were dried in a critical point dryer (Quorum Technologies, E3100). The Eppendorf tubes containing the samples were transferred into the sample holder of dryer filled with anhydrous acetone. The acetone was washed out completely from the chamber by filling up and flushing it with liquid CO<sub>2</sub>. After the complete removal of the acetone, the samples were stored in the chamber filled with liquid CO<sub>2</sub> overnight. The next morning, the chamber was flushed with fresh liquid CO<sub>2</sub> and the system was brought above the supercritical conditions (31.1 °C, 73.9 bar) by heating up the chamber using a heating bath circulator (Julabo CORIO C-B27). The supercritical fluid was allowed to fill all the pores of the assembled nanoparticle structures for 5 min, then the chamber was vented gradually and very slowly. After reaching the ambient pressure, the temperature of the dryer was reduced to room temperature and the aerogels were removed and transferred into glass vials.

**Fabrication of Photoelectrodes:** In order to photoelectrochemically characterize the charge carrier transport inside the gel structures, the gels were immobilized on conductive indium tin oxide (ITO) coated glass slides. Firstly, the conductive ITO substrate (VisionTek Ltd., 12 Ω sq<sup>-1</sup>) was cut into 1.5 cm × 3 cm rectangles and their surface were modified with MPTMS as a linker to enhance the number of immobilized nanoparticles on the surface. Prior to the functionalization step, the ITO glass slides were cleaned by immersion into a 5:1:1 v/v/v% water:hydrogen peroxide:ammonia solution at 50 °C for 2 h. Subsequently, the slides were functionalized in a toluene solution containing 1 v/v% of MPTMS at 50 °C for 2 h. Second, a mold was prepared by immobilizing a plastic cuvette on the top of the ITO substrate using silicone glue. The aqueous NP solution was introduced into the cuvette (300 µL) followed by the addition of the Y<sup>3+</sup> or Yb<sup>3+</sup> solution in the desired concentration. The solution was homogenized in the cuvette by means of a pipette and let sit for 17 h. Subsequently, the precipitates were washed with MilliQ

water as described in the washing process of the hydrogels. After the complete drying at ambient conditions ( $20 \pm 1$  °C,  $42 \pm 2\%$  relative humidity,  $\approx 5$  days), the cuvette mold was removed gently with a scalpel to obtain the NP xerogels on the conductive substrate (see Figure S21, Supporting Information, for the optical spectrum and the physical appearance of the photoelectrode).

**Optical Characterization of the Self-Assembled Superstructures:** Dilute nanoparticle solutions (in organic solvent or water) and hydrogels were characterized spectroscopically in semi-micro (4 mm path length) and micro (2 mm path length) quartz cuvettes, respectively. The optical measurements of solid samples (aerogels) were carried out using Teflon sample holders (1 cm in diameter, 3 mm in depth) covered with quartz coverslips. The absorption spectra and PL quantum yields were obtained by a Quanta- $\phi$  integrating sphere coupled to a Horiba Dual-FL spectrofluorometer, the PL spectra and the lifetime measurements (time-correlated single photon counting, TCSPC) were carried out using a Horiba Fluoromax-4 spectrofluorometer equipped with a Horiba NanoLED light source and Fluorohub controlling system ( $\lambda_{\text{exc}} = 454$  nm).

**Structural Characterization of the Self-Assembled Systems:** The SEM and TEM images were taken by a JEOL JSM-6700F (operated at 2 kV) scanning electron microscope and a FEI Tecnai G2 F20 TMP (operated at 200 kV) transmission electron microscope, respectively. SEM samples were obtained by immobilizing pieces of aerogels on conductive carbon tapes. Copper grids, covered with carbon layer (Quantifoil) were used for preparing the TEM samples by drop-casting nanoparticle solutions or hydrogels, or by pulling the grids on the surface of the aerogels gently.

**Photoelectrochemical Measurements:** For all photoelectrochemical measurements, a setup comprised of a ModuLab XM ECS potentiostat (Solartron Analytical), a 7270 DSP lock-in amplifier (Signal Recovery), a HMF2550 arbitrary generator (Rohde&Schwarz), and different commercially available light emitting diodes (5 mm diameter) was employed (the spectra of the diodes can be seen in Figure S20a, Supporting Information). The photon flux of the LEDs (Figure S20b, Supporting Information) was determined with a FDS100 Si photodiode (THORLABS). All measurements were carried out in a self-built measurement cell<sup>[51]</sup> applying a Ag/AgCl reference electrode (3 M NaCl, purchased from BASi) and a roughened platinum wire as the counter electrode. As electrolyte, a 0.5 M aqueous sodium sulfite solution (pH = 9) was used throughout all experiments.

**Linear sweep voltammetry (LSV):** LSVs were recorded under alternating on-off illumination ( $\lambda_{\text{max}} = 472$  nm,  $f = 40$  mHz) with a scanning speed of  $4 \text{ mV s}^{-1}$  in the potential range between  $-600$  and  $300$  mV (versus Ag/AgCl).

**Intensity modulated photocurrent spectroscopy (IMPS):** Over the course of the IMPS experiments, the photon flux of the LED was modulated with a sine wave function. The frequency of the sine wave function was varied in the range between 10 kHz and 1 Hz. In the applied frequency range, the photon flux of the respective LED is nearly independent from the frequency (Figure S20b, Supporting Information). Unless otherwise stated, all IMPS responses were recorded at a bias potential of 150 mV (versus Ag/AgCl).

**X-Ray Photoelectron Spectroscopy:** The samples were analyzed by a SPECS XPS device equipped with a PHILOBOS 100 analyzer and an MCD-5 detector. The measurements were done with a pass energy of 20 eV and an Al K $\alpha$  X-ray beam as excitation source. Aqueous solution of MPA-stabilized shorter CdSe/CdS nanorods ( $c_{\text{Cd}} = 3.6 \text{ g L}^{-1}$ ) was used as reference system: the supernatant and the precipitate have been collected after centrifuging the solution in a centrifuge filter (Sartorius, MW cut off 30.000 Da). The supernatant and the precipitate have been drop-casted onto Si substrate (15 mm  $\times$  7 mm) and dried at ambient conditions. Two other portions of the same initial aqueous nanorod solution have been mixed with YCl $_3$ ·6H $_2$ O and YbCl $_3$ ·6H $_2$ O in the concentration of 10 mM. After the assembly took place, the samples have been centrifuged and the supernatants and precipitates have been collected. All the measured binding energies were calibrated using the measured C 1s peak (284.65 eV).

## Supporting Information

Supporting Information is available from the Wiley Online Library or from the author.

## Acknowledgements

The authors would like to acknowledge the financial support of the German Federal Ministry of Education and Research (BMBF) within the framework of the program NanoMatFutur, support code 03X5525. Furthermore, the project leading to these results has in part received funding from the European Research Council (ERC) under the European Union's Horizon 2020 research and innovation program (grant agreement 714429). In addition, this work was funded by the German Research Foundation (Deutsche Forschungsgemeinschaft, DFG) under Germany's excellence strategy within the cluster of excellence PhoenixD (EXC 2122, project ID 390833453) and the grant BI 1708/4-1. A.S. is thankful for financial support from the Hannover School for Nanotechnology (hsn). The authors moreover thank Armin Feldhoff and Jürgen Caro for providing the SEM facility, and the LNQE for providing the TEM.

## Conflict of Interest

The authors declare no conflict of interest.

## Keywords

functional aerogels, multifunctional 3D networks, nanocrystals, photoelectrochemical sensing, solvogels, semiconductor nanoparticles, trivalent cations

Received: November 27, 2019

Revised: February 17, 2020

Published online:

- [1] L. Polavarapu, S. Mourdikoudis, I. Pastoriza-Santos, J. Pérez-Juste, *CrystEngComm* **2015**, *17*, 3727.
- [2] A. Schlosser, L. C. Meyer, F. Lübckemann, J. F. Miethe, N. C. Bigall, *Phys. Chem. Chem. Phys.* **2019**, *21*, 9002.
- [3] Y. Lou, Y. Zhao, J. Chen, J.-J. Zhu, *J. Mater. Chem. C* **2014**, *2*, 595.
- [4] J. N. Freitas, A. S. Gonçalves, A. F. Nogueira, *Nanoscale* **2014**, *6*, 6371.
- [5] V. L. Bridewell, R. Alam, C. J. Karwacki, P. V. Kamat, *Chem. Mater.* **2015**, *27*, 5064.
- [6] F. Qiu, Z. Han, J. J. Peterson, M. Y. Odoi, K. L. Sowers, T. D. Krauss, *Nano Lett.* **2016**, *16*, 5347.
- [7] R. Bera, A. Dutta, S. Kundu, V. Polshettiwar, A. Patra, *J. Phys. Chem. C* **2018**, *122*, 12158.
- [8] A. S. Karakoti, R. Shukla, R. Shanker, S. Singh, *Adv. Colloid Interface Sci.* **2015**, *215*, 28.
- [9] C. J. Murphy, *Anal. Chem.* **2002**, *74*, 520 A.
- [10] T. K. Kormilina, S. A. Cherevkov, A. V. Fedorov, A. V. Baranov, *Small* **2017**, *13*, 1702300.
- [11] D. Zámbo, G. Z. Radnóczy, A. Deák, *Langmuir* **2015**, *31*, 2662.
- [12] D. Zámbo, S. Pothorszky, D. F. Brougham, A. Deák, *RSC Adv.* **2016**, *6*, 27151.
- [13] I. K. Hewavitharana, S. L. Brock, *Z. Für Phys. Chem.* **2018**, *232*, 1691.
- [14] V. Lesnyak, A. Wolf, A. Dubavik, L. Borchardt, S. V. Voitekhovich, N. Gaponik, S. Kaskel, A. Eychmüller, *J. Am. Chem. Soc.* **2011**, *133*, 13413.

- [15] E. K. Fox, F. El Haddassi, J. Hierrezuelo, T. Ninjbadgar, J. K. Stolarczyk, J. Merlin, D. F. Brougham, *Small* **2018**, *14*, 1802278.
- [16] L. J. A. Koster, S. Khodabakhsh, N. C. Greenham, *Soft Matter* **2014**, *10*, 6485.
- [17] L. Carbone, C. Nobile, M. De Giorgi, F. D. Sala, G. Morello, P. Pompa, M. Hytch, E. Snoeck, A. Fiore, I. R. Franchini, M. Nadasan, A. F. Silvestre, L. Chiodo, S. Kudera, R. Cingolani, R. Krahné, L. Manna, *Nano Lett.* **2007**, *7*, 2942.
- [18] T. Paik, B. T. Diroll, C. R. Kagan, C. B. Murray, *J. Am. Chem. Soc.* **2015**, *137*, 6662.
- [19] A. Freytag, S. Sánchez-Paradinas, S. Naskar, N. Wendt, M. Colombo, G. Pugliese, J. Poppe, C. Demirci, I. Kretschmer, D. W. Bahnemann, P. Behrens, N. C. Bigall, *Angew. Chem., Int. Ed.* **2016**, *55*, 1200.
- [20] A. Freytag, M. Colombo, N. C. Bigall, *Z. Für Phys. Chem.* **2017**, *231*, 63.
- [21] T. Gacoin, L. Malier, J.-P. Boilot, *J. Mater. Chem.* **1997**, *7*, 859.
- [22] T. Gacoin, L. Malier, J.-P. Boilot, *Chem. Mater.* **1997**, *9*, 1502.
- [23] N. C. Bigall, A.-K. Herrmann, M. Vogel, M. Rose, P. Simon, W. Carrillo-Cabrera, D. Dorfs, S. Kaskel, N. Gaponik, A. Eychmüller, *Angew. Chem., Int. Ed.* **2009**, *48*, 9731.
- [24] N. C. Bigall, A. Eychmüller, *Philos. Trans. R. Soc., A* **2010**, *368*, 1385.
- [25] W. Liu, A.-K. Herrmann, N. C. Bigall, P. Rodriguez, D. Wen, M. Oezaslan, T. J. Schmidt, N. Gaponik, A. Eychmüller, *Acc. Chem. Res.* **2015**, *48*, 154.
- [26] D. Wen, W. Liu, D. Haubold, C. Zhu, M. Oschatz, M. Holzschuh, A. Wolf, F. Simon, S. Kaskel, A. Eychmüller, *ACS Nano* **2016**, *10*, 2559.
- [27] D. Wen, A. Eychmüller, *Chem. Commun.* **2017**, *53*, 12608.
- [28] C. Ziegler, A. Wolf, W. Liu, A.-K. Herrmann, N. Gaponik, A. Eychmüller, *Angew. Chem., Int. Ed.* **2017**, *56*, 13200.
- [29] B. Cai, V. Sayevich, N. Gaponik, A. Eychmüller, *Adv. Mater.* **2018**, *30*, 1707518.
- [30] S. Sánchez-Paradinas, D. Dorfs, S. Friebe, A. Freytag, A. Wolf, N. C. Bigall, *Adv. Mater.* **2015**, *27*, 6152.
- [31] S. Naskar, J. F. Miethe, S. Sánchez-Paradinas, N. Schmidt, K. Kanthasamy, P. Behrens, H. Pfnür, N. C. Bigall, *Chem. Mater.* **2016**, *28*, 2089.
- [32] Y. Yan, L. Wang, C. B. Vaughn, G. Chen, P. G. Van Patten, *J. Phys. Chem. C* **2011**, *115*, 24521.
- [33] Q. Yao, S. L. Brock, *Inorg. Chem.* **2011**, *50*, 9985.
- [34] S. F. Wuister, C. de Mello Donegá, A. Meijerink, *J. Phys. Chem. B* **2004**, *108*, 17393.
- [35] S. F. Wuister, I. Swart, F. van Driel, S. G. Hickey, C. de Mello Donegá, *Nano Lett.* **2003**, *3*, 503.
- [36] T. Kodanek, H. M. Banbela, S. Naskar, P. Adel, N. C. Bigall, D. Dorfs, *Nanoscale* **2015**, *7*, 19300.
- [37] N. Shambetova, Y. Chen, H. Xu, L. Li, J. Solandt, Y. Zhou, J. Wang, H. Su, H. Brismar, Y. Fu, *J. Phys. Chem. C* **2016**, *120*, 3519.
- [38] N. Bel Haj Mohamed, N. Ben Brahim, R. Mrad, M. Haouari, R. Ben Chaâbane, M. Negreie, *Anal. Chim. Acta* **2018**, *1028*, 50.
- [39] R. K. Sajwan, Y. Bagbi, P. Sharma, P. R. Solanki, *J. Lumin.* **2017**, *187*, 126.
- [40] J. Ke, X. Li, Q. Zhao, Y. Hou, J. Chen, *Sci. Rep.* **2015**, *4*, 5624.
- [41] J.-L. Chen, C.-Q. Zhu, *Anal. Chim. Acta* **2005**, *546*, 147.
- [42] M. A. Boles, D. Ling, T. Hyeon, D. V. Talapin, *Nat. Mater.* **2016**, *15*, 364.
- [43] Z. Lingley, S. Lu, A. Madhukar, *Nano Lett.* **2011**, *11*, 2887.
- [44] J. P. Vanegas, J. C. Scaiano, A. E. Lanterna, *Langmuir* **2017**, *33*, 12149.
- [45] P. Rusch, B. Schremmer, C. Strelow, A. Mews, D. Dorfs, N. C. Bigall, *J. Phys. Chem. Lett.* **2019**, *10*, 7804.
- [46] Y.-J. Liang, F. Liu, Y.-F. Chen, X.-J. Wang, K.-N. Sun, Z. Pan, *Light: Sci. Appl.* **2016**, *5*, e16124.
- [47] J. P. Vanegas, E. Zaballos-García, M. González-Béjar, P. Londoño-Larrea, J. Pérez-Prieto, *RSC Adv.* **2016**, *6*, 17678.
- [48] F. Lübke, J. F. Miethe, F. Steinbach, P. Rusch, A. Schlosser, D. Zámbo, T. Heinemeyer, D. Natke, D. Zok, D. Dorfs, N. C. Bigall, *Small* **2019**, *15*, 1902186.
- [49] S. G. Hickey, D. J. Riley, *Electrochim. Acta* **2000**, *45*, 3277.
- [50] J. F. Miethe, F. Lübke, A. Schlosser, D. Dorfs, N. C. Bigall, *Langmuir*, **2020**.
- [51] J. F. Miethe, F. Lübke, J. Poppe, F. Steinbach, D. Dorfs, N. C. Bigall, *ChemElectroChem* **2018**, *5*, 175.
- [52] W. W. Yu, L. Qu, W. Guo, X. Peng, *Chem. Mater.* **2003**, *15*, 2854.
- [53] M. D. Tessier, P. Spinicelli, D. Dupont, G. Patriarche, S. Ithurria, B. Dubertret, *Nano Lett.* **2014**, *14*, 207.
- [54] R. García-Rodríguez, H. Liu, *J. Am. Chem. Soc.* **2012**, *134*, 1400.
- [55] B. Abécassis, M. D. Tessier, P. Davidson, B. Dubertret, *Nano Lett.* **2014**, *14*, 710.
- [56] S. Pedetti, S. Ithurria, H. Heuclin, G. Patriarche, B. Dubertret, *J. Am. Chem. Soc.* **2014**, *136*, 16430.